Journal of Molecular Liquids 413 (2024) 125998

Contents lists available at ScienceDirect

Journal of Molecular Liquids

journal homepage: www.elsevier.com/locate/molliq

Combining in-situ quadrupole mass spectrometer analyses: Study on the structure–activity relationship and lubrication mechanisms of ammonium phosphate ionic liquids

Guanai Qu [a,b], Hongling Fang [a,b], Yi Li [a,c], Songwei Zhang [a,c,*], Litian Hu [a,**]

[a] State Key Laboratory of Solid Lubrication, Lanzhou Institute of Chemical Physics, Chinese Academy of Sciences, Lanzhou 730000, PR China
[b] Center of Materials Science and Optoelectronics Engineering, University of Chinese Academy of Sciences, Beijing 100049, PR China
[c] Qingdao Center of Resource Chemistry & New Materials, Qingdao 266071, PR China

ARTICLE INFO

Keywords:
Protic ionic liquids
Quadrupole mass spectrometer
Intermolecular forces
Lubrication mechanism
Vacuum

ABSTRACT

Since the lubrication performances of ionic liquids are closely linked to their unique structures, four protic ionic liquids (PILs), [N_{44}HH][DEHP], [N_{444}H][DEHP], [N_{448}H][DEHP] and [N_{4412}H][DEHP], are designed to investigate the effect of cationic structures on the lubrication behaviors and lubrication mechanisms. Vacuum tribological tests were carried out to minimize the impact of the atmospheric environment. The structure–activity relationships and lubrication mechanisms of PILs were emphatically examined by in-situ quadrupole mass spectrometer (Q-MS) and XPS analyses. Results demonstrated that all four PILs exhibited outstanding lubrication performance under a vacuum condition. Unusually, extended alkyl chain cationic structures resulted in a changed lubrication mechanism, leading to a slight decrease in performance. In-situ Q-MS analyses and XPS further revealed that the length of the alkyl chain in cations influenced the strength of intermolecular forces in PILs, leading to changes in their lubrication performance and mechanisms.

1. Introduction

The loss of energy, materials, and money due to friction and wear between contact surfaces has afflicted many industries worldwide [1,2]. To address these issues, the utilization of lubricants in a sensible manner can significantly reduce these losses. However, using lubricants presents various challenges in terms of reducing friction and wear, as well as minimizing pollution. Therefore, it is vital to develop more advanced lubricants to address these challenges effectively. Ionic liquids (ILs) are exciting lubricant materials for their unique physicochemical properties and design flexibility [3,4], allowing them to be used in harsh environments. In 2001, ILs were internationally recognized as a new type of lubricant with excellent lubricating properties [5]. The following year, the IL of alkylimidazolium tetrafluoroborate was evaluated in a vacuum and found to have superior lubricating properties compared to commonly used lubricants in space [6,7]. Through further research, ILs have gained recognition as lubricating materials, primarily employed in ground environments as pure lubricants or additives in base oils for various friction and wear conditions.

The ILs currently used in experiments that exhibit excellent lubrication performance mainly consist of cations containing alkylimidazoles and anions containing halogen [8–11]. However, the halogen-containing anions can cause severe corrosion to metal substrates and do not meet green requirements. It is necessary to find and synthesize ILs that can be used in harsh conditions without halogens. Among these ILs, the bis(2-ethylhexyl) phosphate (DEHP)-based ILs have been extensively studied and shown excellent performance [12–16]. Although the varieties and quantities of ionic liquids (ILs) with excellent tribological properties are rapidly increasing in the field of friction, it is worth conducting in-depth studies on the structure–activity relationship and lubrication mechanisms of ILs with similar structures. In addition, the designability of ILs' structures allows them to be widely applied in multiple fields by introducing the required structure into ILs [17]. Therefore, we have designed four PILs, [N_{44}HH][DEHP], [N_{444}H][DEHP], [N_{448}H][DEHP], [N_{4412}H][DEHP] to investigate the lubrication mechanisms of ILs by varying the cationic structures. The

* Corresponding author at: State Key Laboratory of Solid Lubrication, Lanzhou Institute of Chemical Physics, Chinese Academy of Sciences, Lanzhou 730000, PR China.
** Corresponding author.
E-mail addresses: zhangsw@licp.cas.cn (S. Zhang), lthu@licp.cas.cn (L. Hu).

https://doi.org/10.1016/j.molliq.2024.125998
Received 24 June 2024; Received in revised form 23 August 2024; Accepted 11 September 2024
Available online 14 September 2024

morphology and composition of worn surfaces are usually used to analyze the investigation of the structure–activity relationship between lubrication performances and IL structures [18–20].

In this paper, in order to minimize the influence of environmental factors, we conducted friction experiments under high vacuum conditions in this study. In addition to the XPS analyses on worn surfaces, the in-situ quadrupole mass spectrometer (Q-MS) was combined to conduct the degradation debris of PILs. The results of the friction experiments showed that four PILs exhibited exceptional lubrication performance in a vacuum. It is important to note, however, that there was a change in physicochemical properties and a noticeable decline in lubrication performance as the alkyl chain was extended. Therefore, the PILs had significant structure–activity relationships, and the lubrication mechanisms were discussed.

2. Experimental section

2.1. Materials

The reagents in the experimental used as the raw material to synthesize the phosphate-based PILs are as follows: Dibutylamine (Purity ≥99 %) was purchased from Sinopharm Chemical Reagent Co., Ltd, n-butyl bromide (Purity ≥99 %), 1-bromododecane (Purity ≥98 %) and bis (2-ethylhexyl) phosphate (HDEHP) (Purity ≥99 %) were from Shanghai Aladdin Bio-Chem Technology Co., LTD. 1-Bromooctane (Purity ≥99 %) was purchased from Shanghai Macklin Biochemical Co., Ltd, and potassium hydroxide (KOH) (Purity ≥85 %) was from Tianjin Kaitong Chemical Reagent Co., Ltd. All the reagents in the test were without further purification.

2.2. Synthesis of PILs

The synthetic method of $[N_{44}HH][DEHP]$ was simple and environment-friendly, only stirring at room temperature for 12 h. The synthesis of $[N_{44X}H][DEHP]$ was mainly in two separate steps. The first step involved linking the alkyl group to the nitrogen atom of dibutylamine to create the tertiary amine salt $[N_{44X}H][Br]$. The subsequent ion exchange process was used to obtain the target PILs. The specific steps are as follows:

$[N_{44X}H][Br]$: Dibutylamine (0.1 mol) was stored in a 100 mL single distilling flask, and then the 1-bromo-hydrocarbon (0.1 mol) was added dropwise. The mixture was stirred at a temperature of 70–80 °C for 12 h to ensure a complete reaction of the reagents. The product, resembling a white gelatinous substance, was obtained.

$[N_{44X}H][DEHP]$: Potassium hydroxide (KOH) (0.1 mol) and equimolar bis (2-ethylhexyl) phosphate (DEHP) were reacted in absolute alcohol, and the product was a pale yellow liquid. The addition of $[N_{44X}H][Br]$ to the liquid resulted in the formation of the solid white KBr. After stirring for 12 h, the solids were removed by multiple filtrations, and the reaction solvent was removed by rotary evaporation. Finally, the ILs were dried at 70 °C for 12 h in the vacuum drying chamber and obtained the target products. In this paper, three tertiary ammonium PILs were synthesized (X = 4, 8, 12). The synthesis of PILs was confirmed by the Quadrupole Time-of-Flight mass spectrometer in the supplementary material. As shown in Fig. S1a to e, (Q-TOF MS Bruker maXis): MS (Q-TOF positive) $m/z = 130.16$ ($[C_8H_{20}N]^+$), MS (Q-TOF positive) $m/z = 186.22$ ($[C_{12}H_{28}N]^+$), MS (Q-TOF positive) $m/z = 242.28$ ($[C_{16}H_{36}N]^+$), MS (Q-TOF positive) $m/z = 298.35$ ($[C_{20}H_{44}N]^+$) and MS (Q-TOF negative), $m/z = 321.23$ ($[C_{16}H_{34}PO_4]^-$).

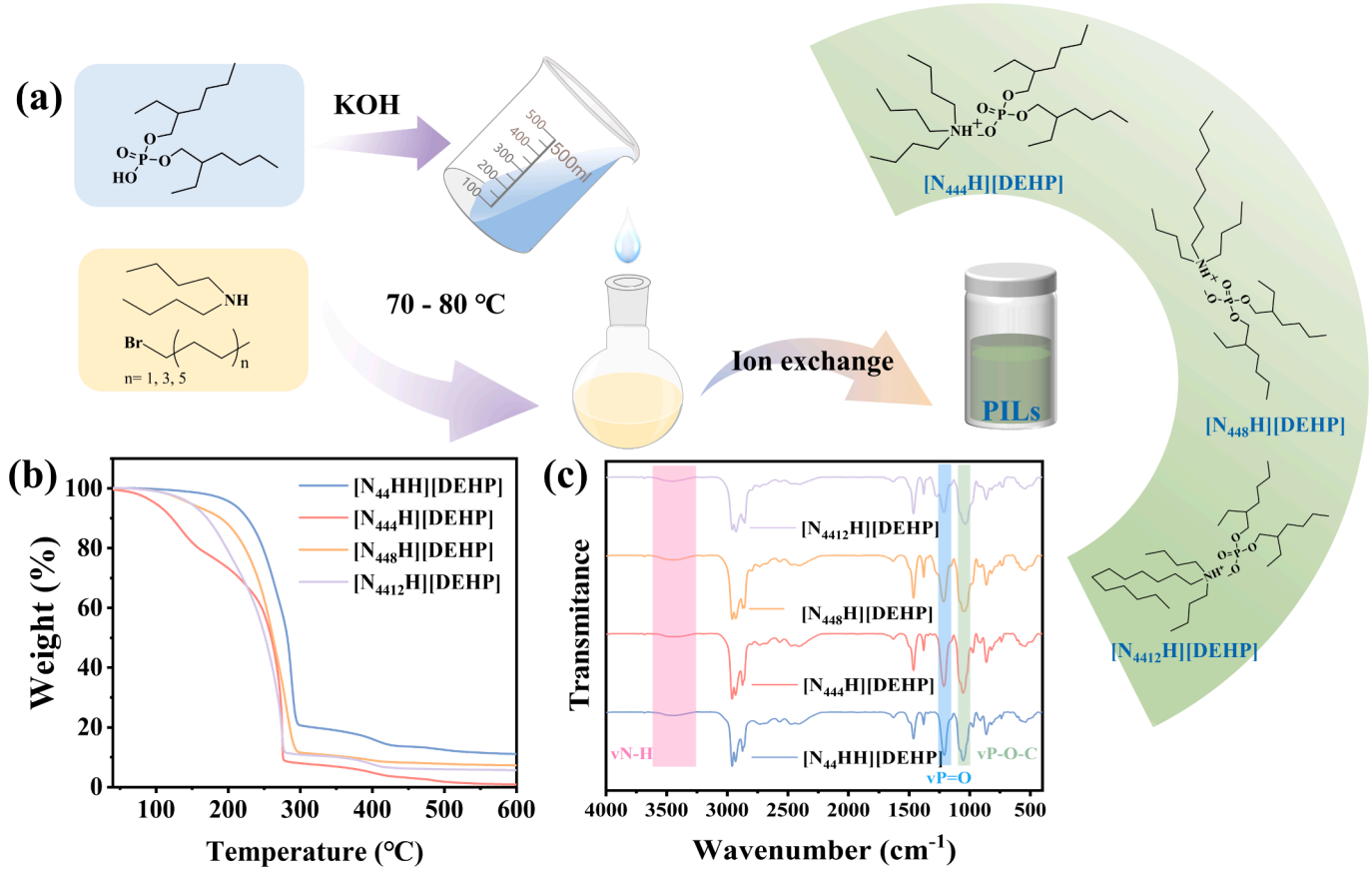

Fig. 1. (a) The chemical structures of cations and anions of PILs in this study. (b) TGA curves of the four PILs. (c) FTIR spectra of PILs ranging from 400 to 4000 cm^{-1}.

2.3. Characterization of ILs and surface

The chemical structures of four PILs were displayed in Fig. 1a, and the structures were proved by Q-TOF MS (MS Bruker-maXis) and Fourier Transform Infrared (FTIR Bruker TENSOR+27) spectroscopy. The kinematic viscosity of four ILs was observed by a kinematic viscosity tester (WZ-265A) at 40 °C and 100 °C. Thermogravimeter analysis (TGA, HITACHI STA200) experimented with a heating rate of 10 °C/min at the temperature range of 40 °C–600 °C, and decomposition temperature was determined in an N_2 atmosphere. The pour point of each PIL was tested to examine their low-temperature fluidity.

The morphology of wear scar surfaces and chemical element composition were obtained by field emission scanning electron microscopy (Model EVO 10, Zeiss, Germany), X-ray photoelectron spectroscopy (XPS, PHI5000 Versaprobe III) was used to detect the chemical states of elements wear scar surfaces and quantitative analysis of wear scar surfaces. In this paper, the calibration reference of the binding energy of the XPS photoelectron spectra is C 1s of 284.80 eV.

2.4. Vacuum friction and tribo-degradation tests

The vacuum friction and tribo-degradation tests were completed by the VFBT-4000 vacuum four-ball tribometer equipped with a Pfeiffer Q-MS. During the friction process, the ILs adsorbed on the interface and protected the substrate, while the IL debris caused by tribo-degradation floated in the cavity was partially collected and detected by Q-MS. The frictional pairs were composed of one upper test ball and three lower test balls, which were GCr15 with a diameter of 12.7000 mm. Each test used 10 mL ILs to ensure three lower steel balls were thoroughly soaked in ILs. All the tests were conducted at room temperature, with a velocity of 1450 ± 10 rpm, and the load was 294 N. All the balls and holders used in the tests were cleaned with petroleum ether and anhydrous alcohol. Each vacuum tribological test was under the pressure of 2.0×10^{-4} Pa, and the friction duration was 30 min. In this work, each group of tests repeated three same-condition tests, and the average wear scar diameter (WSD) calculated the WSD from the tests.

The processes of tribo-degradation were recorded and analyzed by Q-MS trapping fragments. The high vacuum system was constructed through a mechanical pump and turbo molecular pump. To avoid the effect of the background atmosphere, the volatile fragments before and during the friction process were collected, and each period was collected for 8 min. Before the friction process, we needed to manage valid data of the background, I_b (m/z), and standard deviation, σ_b (m/z). Then, we obtained the differential mass spectrometry (DMS) spectra by calculating the following:

$$\Delta I(m/z,t) = I(m/z,t) - \bar{I}_b(m/z)$$

Moreover, DMS spectra showed the changes in each fragment over time caused by friction decomposition. To avoid random variations as much as possible, the DMS spectra were filtered as follows:

$$If[SN(m/z,t)] > 5,\ \Delta I(m/z,t) = I(m/z,t);$$

$$If[SN(m/z,t)] \leqslant 5,\ \Delta I(m/z,t) = 0.$$

In the prerequisite conditions, SN (m/z, t) = I (m/z, t)/ σ_b (m/z). It means the signal-to-noise ratio of the relevant mass component in the DMS spectra at a particular moment [21].

3. Results and discussion

3.1. Physicochemical properties

Compared with [N_{44}HH][DEHP], the significant difference for the other PILs is the addition of an alkyl chain to the nitrogen atom, making them a tertiary amine salt. This change also resulted in a decrease in the number of protic hydrogen atoms. In Fig. 1c, the FTIR analysis shows that a broad peak at 3500–3000 cm^{-1} corresponds to the stretching vibration of N^+—H in four PILs. Another broad peak in the range of 3500–2200 cm^{-1} is the ammonium band, which relates to the stretching vibration of C—H. Additionally, all the PILs in this study share the same phosphate ester anion. The stretching vibration absorption of P═O is observed in a wide range from 1150–1310 cm^{-1}. The P—O—C bonds in fatty organophosphorus compounds exhibit a strong to moderate broad peak around 1050 cm^{-1}. Since these four PILs have similar functional groups, no significant differences can be observed in the infrared spectra.

The thermal stability of ILs is limited by interactions between heteroatoms and carbon atoms, as well as hydrogen bonds, which are closely related to the structures and properties of their cations and anions. [N_{44}HH][DEHP] with short carbon chains has stronger hydrogen bonding interactions, with hydrogen bonding dominating. Therefore, [N_{44}HH][DEHP] has better thermal stabilization compared to the other three PILs due to the dominant role of rich protic hydrogen. From Fig. 1b, it is clear that an increase in the alkyl chain affects PILs' thermal stability [22]. For the other three PILs, the length of one alkyl chain is incrementally increased by adding four carbon atoms. Among them, [N_{444}H][DEHP] has the worst thermal stability, while [N_{448}H][DEHP] is marginally better than [N_{4412}H][DEHP]. The rule that the cations with longer the alkyl chains, the better the thermal stability is only partially applicable.

When ILs are used as lubricant oils, a low pour point often indicates a low melting point. Generally, ILs with low melting points are characterized by low symmetry in their cations, weak intermolecular forces, and a uniform distribution of cation charges. In other words, the more dispersed the charge in the cation, the lower the molecular symmetry and the lower the melting point of the resulting ILs [23]. Table 1 compares the physico-chemical properties of four PILs, including viscosity, viscosity index, TG temperature (°C) per weight loss, and pour points of PILs. From Table 1, it is evident that the pour points of [N_{448}H][DEHP] and [N_{4412}H][DEHP] are obviously lower than [N_{444}H][DEHP]. When [N_{444}H][DEHP] has changed from liquid into solid, [N_{448}H][DEHP] and [N_{4412}H][DEHP] still maintain excellent fluidity. The long alkyl chain increases the asymmetric geometry of the ammonium cation, impeding the interactions between cations and anions [24]. At the same time, this decreases the Van der Waals force, which is in line with the original intention of the structural design for [N_{448}H][DEHP] and [N_{4412}H][DEHP]. Therefore, the method of increasing a single chain was great for declining the pour point of ILs, which could increase the application of ILs in the field of low-temperature lubrication engineering. In the case of [N_{44}HH][DEHP], hydrogen bonding interaction is dominant in intermolecular force. [N_{444}H][DEHP] with same-length alkyl chains on the ammonium cation reinforces the geometric symmetry, which weakens the hydrogen bonding interaction. As a result, although [N_{444}H][DEHP], [N_{448}H][DEHP], and [N_{4412}H][DEHP] have the same anions and similar cations, the intermolecular forces are more influenced by molecular symmetry. The kinematic viscosity value of [N_{44}HH][DEHP] is the

Table 1
The viscosity, viscosity index, TG temperature (°C) per weight loss, and pour points of PILs.

Lubricants	Kinematic viscosity/mm^2/s		Viscosity index	TG temperature per weight loss/ °C		Pour points/ °C
	40 °C	100 °C		5 %	10 %	
[N_{44}HH][DEHP]	368.69	44.23	177	205.34	226.46	−10
[N_{444}H][DEHP]	332.57	35.38	152	99.08	122.10	−34
[N_{448}H][DEHP]	25.59	4.97	121	147.46	189.67	−70
[N_{4412}H][DEHP]	33.03	5.97	127	147.68	170.76	−53

largest among them, followed by [N_{444}H][DEHP], [N_{4412}H][DEHP], and [N_{448}H][DEHP]. Viscosity is influenced by a combination of Van der Waals force and hydrogen bonding, with the effect of hydrogen bonding being very pronounced. Therefore, [N_{44}HH][DEHP] with strong hydrogen bonding has a higher viscosity, while [N_{448}H][DEHP] with strong molecular asymmetry has a lower viscosity.

3.2. Vacuum friction and wear properties of ILs

Fig. 2 presents the vacuum lubrication performances of four PILs at a high vacuum. The anti-friction and anti-wear performance of PILs are reflected by friction coefficient (COF) and wear scar diameter (WSD), respectively. As shown in Fig. 2a, the friction curves of four PILs are relatively stable throughout the whole process, and the COF is as low as approximately 0.62. From Fig. 2b, it is evident that the anti-friction and anti-wear performance of [N_{448}H][DEHP] and [N_{4412}H][DEHP] are slightly worse than [N_{44}HH][DEHP] and [N_{444}H][DEHP]. Nevertheless, the four PILs have good lubrication properties under high vacuum and load conditions.

Scanning electron microscopy (SEM) was used to analyze the surface topography of the wear scars to explore the tribological properties of the ILs further. SEM images included full view and partial enlargement of the wear scars. As shown in Fig. 2c–j, the edge of the wear scar has apparent plastic deformation and furrow, while the wear surface of [N_{444}H][DEHP] is shallow without severe wear. It meant that the [N_{44}HH][DEHP] and [N_{444}H][DEHP] effectively protected the steel surface and reduced the surface damage. The wear scar lubricated with [N_{448}H][DEHP] was the largest among these worn surfaces. From Fig. 2e and f, the slight adhesive wear on the worn surface is covered by an oxide film-like substance. The wear scar of [N_{4412}H][DEHP] was a little less than [N_{448}H][DEHP], but the furrow was evident on the surface from Fig. 2j.

3.3. Vacuum tribo-decomposition behaviors of PILs

The chemical bonds between organic molecules can be broken by external factors such as friction, pressure, and temperature. These factors can cause mechanical and chemical degradation, with frictional degradation being the most common form of mechanical degradation [25]. During friction processing, the sliding of frictional subsets generates localized high temperatures, high pressure, and shear forces. These mechanical energies stimulate the chemical bonds within organic molecules. Frictional work generates heat, increasing the temperature, but the temperature elevation is significantly lower than the energy required to initiate thermochemical reactions. Consequently, we attempted to obtain the debris from the friction processes using in-situ MS for analysis.

The DMS spectra of ILs during the friction processes are presented in Fig. 3a–d, with the error bars indicating standard deviation (σ). Due to the overlapping ionic fragments of different volatile products, it is hard to accurately identify all volatile spectral components in the decomposition products of IL molecules. Although the process of friction decomposition is not quite the same as the ionization of an ion source for conventional mass spectrometry, the fragmentation mechanism could be roughly inferred from the conventional ionization. In this work, the main cleavage modes of the cations from ILs were α-break and σ-break, producing $NH_xC_yH_z^+$ fragments centered on nitrogen atoms and alkyl fragments of different carbon atom numbers [26]. In addition to the two ways of fragmentation of the cations mentioned above, there was also heterolytic bond cleavage i-break. As is shown in Fig. 3e, the main possible frictional fragmentation mechanisms of cations are displayed, and more fragmentation pathways are not entirely shown. Due to the overlapping ionic fragments of different volatile products, accurately identifying all volatile spectral components in the decomposition products of IL molecules is challenging.

The peaks of m/z 14–16 were mainly vested in CH_n^+ (n = 2–4). These

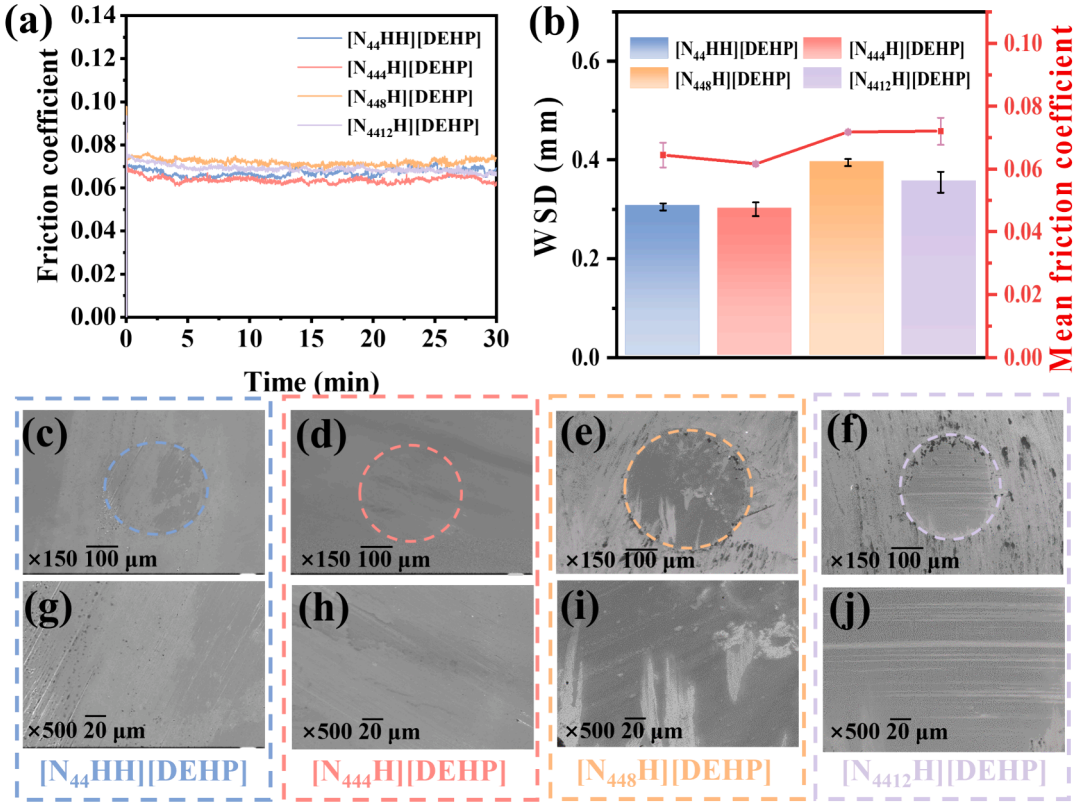

Fig. 2. The vacuum lubrication performances of four PILs: (a) The friction coefficient curves as functions of time. (b) WSD and mean friction coefficient. The SEM images of full view and partial enlargement wear scars: (c, g) [N_{44}HH][DEHP], (d, h) [N_{444}H][DEHP], (e, i) [N_{448}H][DEHP], (f, j) [N_{4412}H][DEHP].

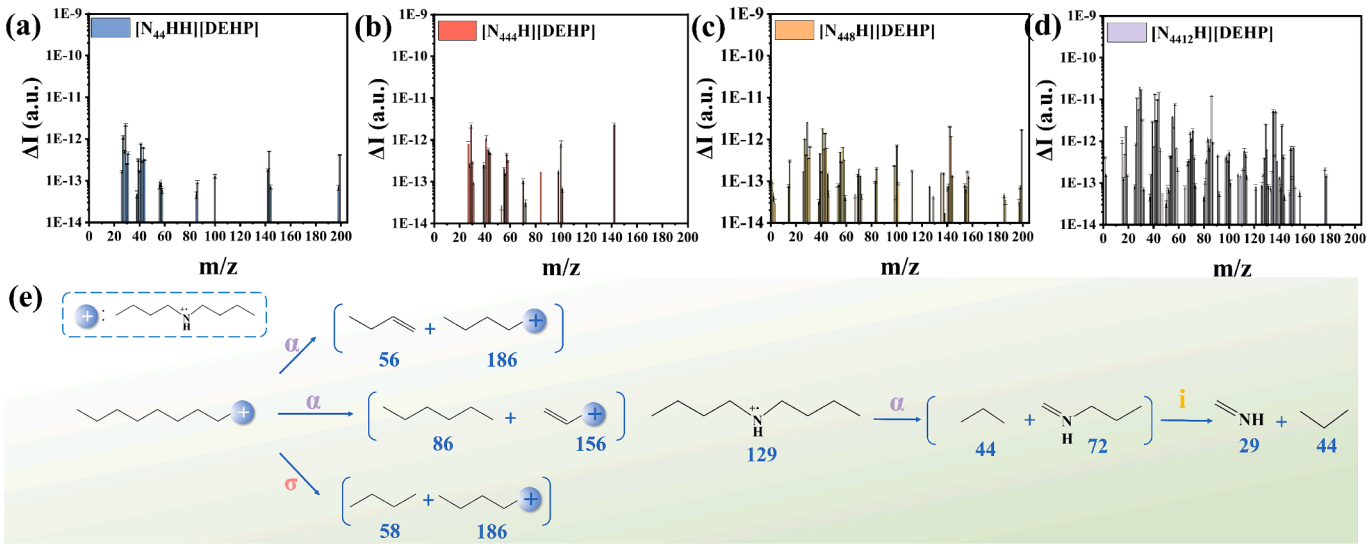

Fig. 3. DMS spectra for four PILs during the friction processes: (a) [N_{44}HH][DEHP], (b) [N_{444}H][DEHP], (c) [N_{448}H][DEHP], (d) [N_{4412}H][DEHP]. (e) The main possible frictional fragmentation mechanisms of cations.

spectral peaks at 26–30, 38–44, 53–58, and 68–72 were determined as the mixture of C2, C3, C4, and C5 alkanes or alkenes fragments. Moreover, the peaks of 28, 31, 44, 45, and 73 were oxygen-containing ion fragments, CO^+, CH_3O^+, CO_2^+, $C_2H_5O^+$, and $C_4H_9O^+$. The peaks at 45, 73, and 142 could also be vested in nitrogen-containing fragments $C_2H_7N^+$, $C_4H_{11}N^+$, and $C_4H_{11}N^+$. Therefore, the peaks of 80–86, 91–92, 126, 154–155, and 186 were nitrogenous fragments. The presentation of a significant value of *m/z* may be due to fewer molecular breaks, leaving the original structure relatively intact, but more likely due to the combination of different molecular fragments overlapping at the time of capture. Only a few oxygen-containing debris were detected, and the fragment containing phosphorus was not obtained. Therefore, it can be assumed that the oxygen-containing fragments were almost all from the anions, but the P element was more inclined to adsorb at the interface. Although the anion branched and had long carbon chains, the friction degradation was not severe. This can be demonstrated by Fig. 3a and b, which show fewer fragments from the friction process. In the case of Fig. 3c and d, the types and strength of peaks are significantly increased with the addition and lengthening of alkyl chains. It was suggested that in addition to the increase in alkyl fragments, there was also a significant increase in nitrogen fragments. Therefore, it was further indicated that the degradation in the friction process mainly came from cationic moieties, and the cations of PILs with long alkyl chains would produce more degradation products.

3.4. Worn surface analysis

The Q-MS can provide information on the decomposition of PILs in the friction processes, but further analyses are needed to understand the role of PILs on the wear surface. Table 2 shows the atomic concentrations of carbon (C), nitrogen (N), oxygen (O), phosphorus (P), and iron (Fe) for four PILs. Both the anions and cations of PILs are adsorbed proportionally, contributing to the protection of the worn surface. To investigate the effect of anions and cations on the interface, the ratio of nitrogen to phosphorus content was compared to determine the extent of cations' involvement in the friction process. As depicted in Fig. 4b, [N_{44}HH][DEHP] has a significantly higher value of N to P compared to the other three PILs. This clearly suggests that the cations of [N_{44}HH][DEHP] play a major role in protecting the steel interface due to its strong intermolecular forces. On the other hand, the other three tertiary ammonium salt-based PILs showed minimal cation participation in the tribological process. This indicates that the involvement of cations is essential for achieving good lubrication performance.

Table 2
Composition results of worn surface measured by XPS.

PILs	Atom concentration/%				
	C 1s	N 1s	Fe 2p	O 1s	P 2p
[N_{44}HH][DEHP]	77.44	4.27	0.99	16.84	0.46
[N_{444}H][DEHP]	76.30	2.29	0.30	19.36	1.76
[N_{448}H][DEHP]	59.11	2.38	4.46	32.11	1.94
[N_{4412}H][DEHP]	56.23	1.78	3.70	34.36	3.93

In this study, phosphorus on the worn surface was derived exclusively from the anion of PILs, and the phosphorus atom content of three tertiary ammonium salt PILs was higher than [N_{44}HH][DEHP]. During the friction process, ILs have a tribochemical reaction with the steel substrate to produce a tribo-film containing Fe, which obviously increases the Fe content on the worn surface. Therefore, the higher the Fe content, the more steel substrate was involved in the tribochemical reaction. On the one hand, lower Fe content resulted in the steel substrate being well protected by the IL adsorption film, with only a small portion of the steel substrate involved in the tribochemical reaction. On the other hand, the oxidation of Fe was effectively inhibited, meaning that a compelling adsorbed lubricating film was formed at the friction interface. From the perspective of Fe atom content, [N_{44}HH][DEHP] and [N_{444}H][DEHP] are relatively small, while the Fe content of [N_{448}H][DEHP] and [N_{4412}H][DEHP] are significantly higher than the other two PILs. The research has presented that the long alkyl chains can shield the charge-transfer effect dramatically, and the partial charge that transfers from the anions to the cations can be shielded. Then, the intermolecular force weakened, causing the anions to carry a more negative charge. [27,28]. The more negative charges were beneficial for the anions to adsorb on the interface. Therefore, the anions of [N_{448}H][DEHP] and [N_{4412}H][DEHP] were more inclined to adsorb on the steel interface. Based on the above analyses, the [N_{448}H][DEHP] and [N_{4412}H][DEHP] reacted with the surface more quickly, forming tribochemical reaction films on the steel substrates.

As shown in Fig. 4, the XPS spectra reveal the chemical states of certain typical elements in tribological products, and Fig. 4a is an example to illustrate the test element. Since these PILs were involved in the friction interface reaction to varying degrees, the binding energy of peak positions in the XPS spectra was not the same and slightly shifted. For the O 1s spectrogram, two distinct characteristic peaks at 531.7–532.3 eV are C—O and P—O bonds, and 530.1–530.7 eV is the

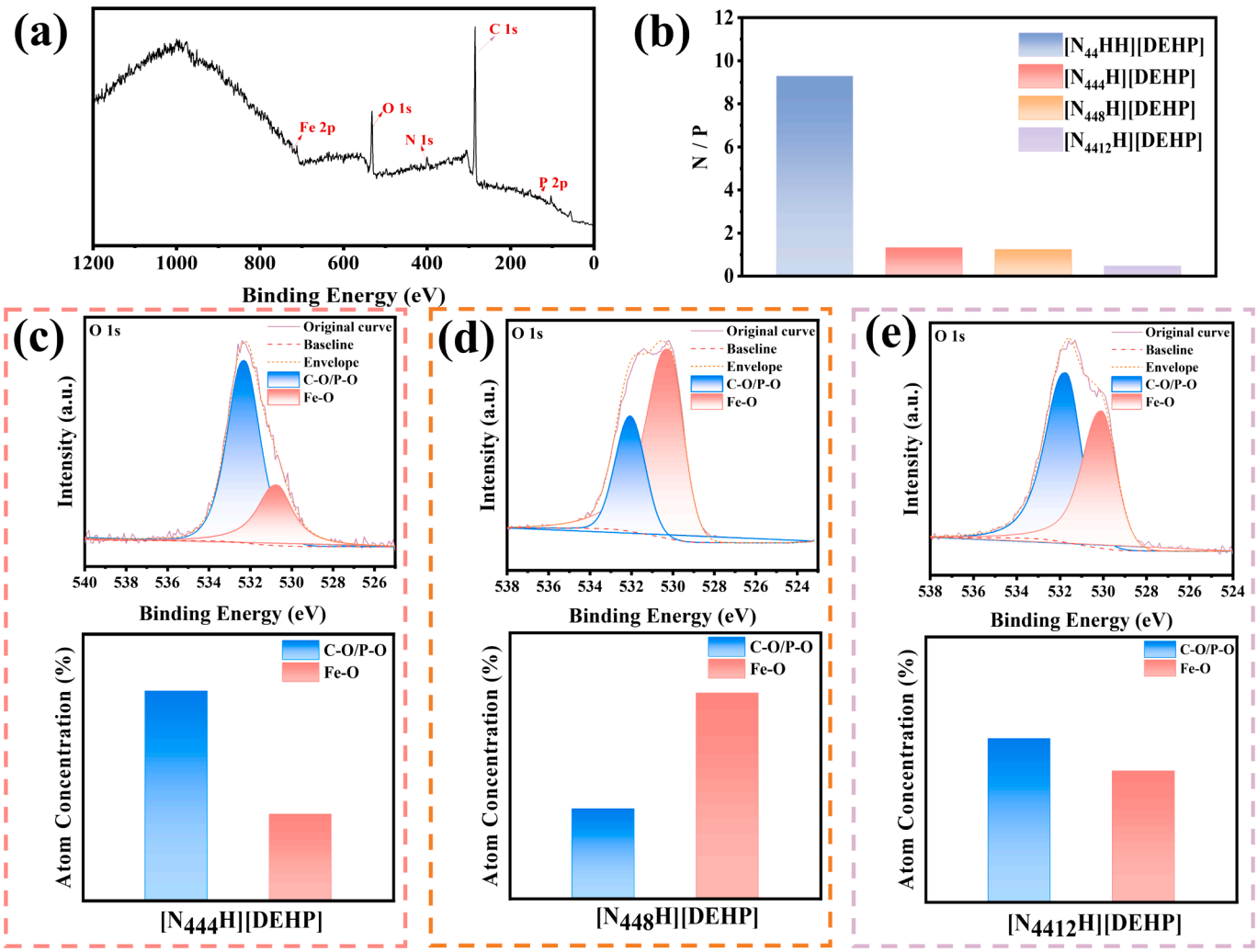

Fig. 4. (a) The general XPS spectrum of [N_{44}HH][DEHP] and the element tested are shown. (b) The nitrogen-phosphorus atom concentration ratios of four PILs. The fitting graph of O 1s and the scaling diagram of the fitted components (c) [N_{444}H][DEHP], (d) [N_{448}H][DEHP], (e) [N_{4412}H][DEHP].

metal oxide bond, like FeO and Fe_2O_3 [29]. The peak of the N 1s spectrogram is only the C—N bond from the cationic skeleton of IL at 399.3–399.9 eV [30,31]. From the P 2p, the binding energy of the P—O bond is 133.5–133.9 eV [13]. To analyze the worn surfaces further, we compared the relative content of the same chemical bond on different surfaces and attempted to explore the friction mechanism of the PILs. As shown in Fig. S2, N 1s of four PILs are from the same chemical bond C—N, which belongs to the cations of PILs. This could imply that the cations were not involved in tribochemical reactions. To further explore the reason for the various lubricant performances in [N_{444}H][DEHP] and [N_{448}H][DEHP], whose nitrogen-phosphorus atom concentration ratios were similar. From the O 1s of XPS spectra, the percentages of C—O/P—O and Fe—O are related to the main composition of the tribofilm and the contribution of the PILs in the friction processes. In the case of Fig. 4c, the C—O/P—O percentage of [N_{444}H][DEHP] exceeds the Fe—O percentage, while the opposite is observed in [N_{448}H][DEHP] as shown in Fig. 4d. It meant that [N_{448}H][DEHP] was more likely to have an intense frictional chemical reaction with the steel surface. As shown in Fig. 4e, the Fe—O percentage of [N_{4412}H][DEHP] increases significantly compared to [N_{444}H][DEHP], but it is lower than [N_{448}H][DEHP]. It is implied that the higher the involvement in the frictional chemical reaction of anions, the worse the lubrication performance; the Fe—O percentage is positively correlated with WSD.

3.5. The lubrication mechanism of four PILs in a vacuum

In order to explore the lubrication mechanism of the PILs in a vacuum, we first calculated the film thickness (h_c) of PILs in a vacuum. The liquid lubricating film thickness between two friction pairs was calculated using the Hamrock-Dowson theory as Eq. [32–34]:

$$h_c = 2.69\frac{G^{0.53}U^{0.67}R}{W^{0.067}}\left(1-0.61e^{-0.73k}\right) \quad (1)$$

$$\frac{2}{E} = \frac{(1-\mu_1^2)}{E_1} + \frac{(1-\mu_2^2)}{E_2} \quad (2)$$

where $G = \alpha E$, $U = \eta\nu/ER$ and $W = F/ER^2$. In this equation, α is the pressure-viscosity coefficient of common ILs ($\alpha \approx 4$ GPa^{-1}) [35–38], ν is the relative sliding linear velocity at 294 N between two steel balls ($\mu_1 = \mu_2 \approx 0.3$), and k is the ellipticity ($k \approx 1$). E is the equivalent elastic modulus of friction pairs, and E_1 is the Elastic modulus of materials on two contact surfaces ($E_1 = E_2 \approx 208$ GPa). The film thickness between friction pairs was calculated, and the approximate results are listed in Table S1. Eventually, [N_{44}HH][DEHP] and [N_{444}H][DEHP] are much higher than [N_{448}H][DEHP] and [N_{4412}H][DEHP], and [N_{448}H][DEHP] has the lowest film thickness.

Therefore, [N_{44}HH][DEHP] and [N_{444}H][DEHP] form a thicker lubricant film to protect the steel surface. Returning to the physicochemical properties of the PILs themselves, the pour point and viscosity

of [N_{448}H][DEHP] and [N_{4412}H][DEHP] were lower than [N_{44}HH][DEHP] and [N_{444}H][DEHP] meant that the intermolecular force of [N_{448}H][DEHP] and [N_{4412}H][DEHP] were weaker. As a result, [N_{448}H][DEHP] and [N_{4412}H][DEHP] molecules were in loose arrangement, causing the formation of poor lubricant films. Flawed lubricant film cannot withstand high loads, leading to easy ruptures and reduced lubrication performance. On the other hand, the cations of [N_{448}H][DEHP] and [N_{4412}H][DEHP] were challenging to adsorb at the interface during friction processes and were mainly captured by Q-MS in the form of volatile fragments due to weak intermolecular interaction. This can be confirmed by the results of XPS and Q-MS, as previously mentioned. Moreover, the long alkyl chain of cations was preferentially cleaved, and the cations tended to form a more stable spatial configuration due to the frictional degradation of cations. Therefore, the viscosity of the PILs in the contact area of the friction pair could increase, and the lubricant state partially shifted to the mixed regime. This can explain why the experimental results of [N_{448}H][DEHP] and [N_{4412}H][DEHP] are worse than [N_{44}HH][DEHP] and [N_{444}H][DEHP], but the lubricant performances of them were still excellent at high load and high vacuum. The lubrication mechanism diagrams of [N_{444}H][DEHP] and [N_{448}H][DEHP] are shown in Fig. 5. The differences between them are due to the strength of the intermolecular forces resulting in lubricant film and the involvement of cations on the interface. For [N_{444}H][DEHP], the stronger anion-cation interactions result in the formation of a more organized and dense PIL film. At the same time, the cations and anions are simultaneously attracted to each other at the interface, collaborating to form an adsorption layer through mutual adsorption. Meanwhile, [N_{448}H][DEHP], due to the single long alkyl chain, reduced the intermolecular force with the loose arrangement of IL film.On the interface, weaker anion-cation interactions allow for more anion adsorption, leading to intense tribochemical reactions that protect the substrate, which causes severe abrasion.

4. Conclusion

In this study, the physicochemical properties and lubrication performances of four PILs with different cationic structures were examined. The in-situ Q-MS collected information on the volatile debris generated during the friction process, and the conclusions are as follows:

(1) The findings indicate that the increase in cationic alkyl chain length reduces the symmetry of the PIL molecules, resulting in alterations to their physicochemical properties, including the reduction of kinetic viscosity and pour point.
(2) The variations in lubrication performance of PILs were primarily caused by cationic moiety, and the shorter alkyl chain length would lead to better lubrication behaviors. XPS results also indicated that strong intermolecular forces in PILs with shorter alkyl chains enhanced the chance of cation involvement in the friction processes.
(3) According to the in-situ Q-MS analyses, the degradation species of PILs during the friction processes mainly came from cationic moieties. Due to weak intermolecular forces, cations with longer alkyl chains are prone to volatilization, producing more degradation debris.
(4) The lubrication mechanisms of PILs are mainly attributed to the fact that cations with shorter alkyl chains exhibit stronger intermolecular forces and tend to form thick and compact adsorption films. Cations with longer alkyl chains exhibit weaker intermolecular forces, and anions easily absorb on worn surfaces, leading to intense tribochemical reactions.
(5) Though extending the cationic alkyl chain will slightly diminish the lubrication performance of ammonium PILs, it is effective in reducing the pour point of PILs, promoting their application in the field of low-temperature lubrication engineering.

CRediT authorship contribution statement

Guanai Qu: Writing – original draft. **Hongling Fang:** Writing – review & editing. **Yi Li:** Data curation. **Songwei Zhang:** Resources. **Litian Hu:** Supervision.

Declaration of competing interest

The authors declare that they have no known competing financial interests or personal relationships that could have appeared to influence the work reported in this paper.

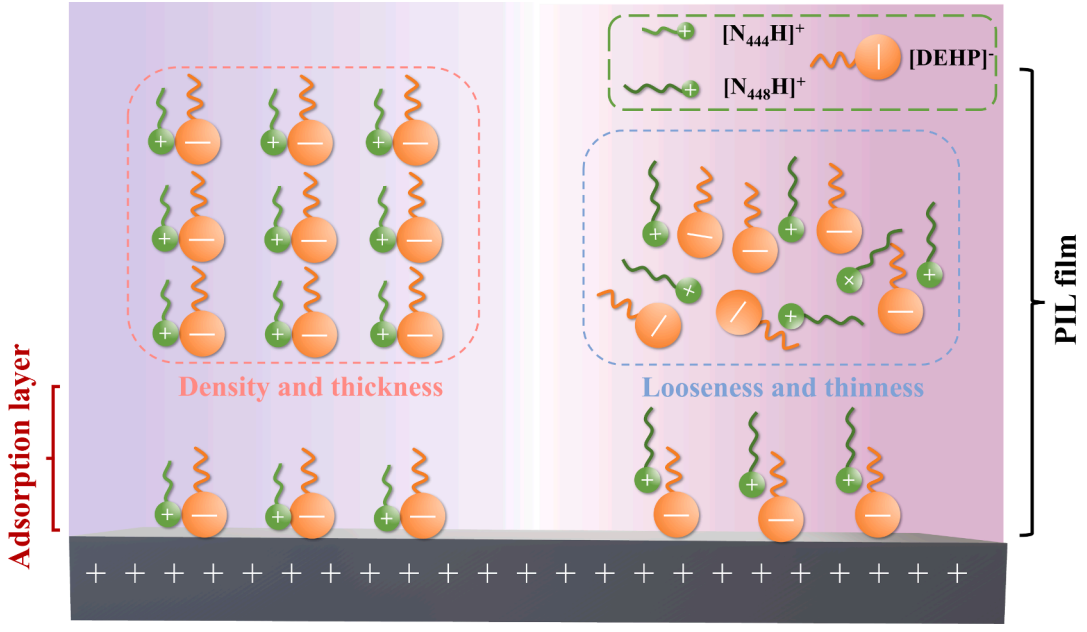

Fig. 5. The schematic diagram of interface adsorption and PIL films of [N_{444}H][DEHP] and [N_{448}H][DEHP].

Data availability

No data was used for the research described in the article.

Acknowledgments

The authors are grateful to the National Natural Science Foundation of China (U21A20280) and Youth Innovation Promotion Association of CAS (2023444).

Appendix A. Supplementary material

Supplementary data to this article can be found online at https://doi.org/10.1016/j.molliq.2024.125998.

References

[1] J. Wang, X. Zhang, S. Zhang, J. Kang, Z. Guo, B. Feng, H. Zhao, Z. Luo, J. Yu, W. Song, S. Wang, Semi-convertible hydrogel enabled photoresponsive lubrication, Matter 4 (2021) 675, https://doi.org/10.1016/j.matt.2020.11.018.
[2] X. Fan, X. Li, Z. Zhao, Z. Yue, P. Feng, X. Ma, H. Li, X. Ye, M. Zhu, Heterostructured rgo/mos_2 nanocomposites toward enhancing lubrication function of industrial gear oils, Carbon 191 (2022) 84, https://doi.org/10.1016/j.carbon.2022.01.037.
[3] Y. Zhou, J. Qu, Ionic liquids as lubricant additives: a review, ACS Appl. Mater. Interfaces 9 (2017) 3209, https://doi.org/10.1021/acsami.6b12489.
[4] P.K. Cooper, C.J. Wear, H. Li, R. Atkin, Ionic liquid lubrication of stainless steel: friction is inversely correlated with interfacial liquid nanostructure, ACS Sustain. Chem. Eng. 5 (2017) 11737, https://doi.org/10.1021/acssuschemeng.7b03262.
[5] C. Ye, W. Liu, Y. Chen, L. Yu, Room-temperature ionic liquids: A novel versatile lubricant, Chem. Commun. 21 (2001) 2244, https://doi.org/10.1039/b106935g.
[6] W. Liu, C. Ye, Q. Gong, H. Wang, P. Wang, Tribological performance of room-temperature ionic liquids as lubricant, Tribol. Lett. 13 (2002) 81.
[7] P. Nancarrow, H. Mohammed, Ionic liquids in space technology - current and future trends, ChemBioEng Rev. 4 (2017) 106, https://doi.org/10.1002/cben.201600021.
[8] A. Suzuki, Y. Shinka, M. Masuko, Tribological characteristics of imidazolium-based room temperature ionic liquids under high vacuum, Tribol. Lett. 27 (2007) 307, https://doi.org/10.1007/s11249-007-9235-8.
[9] R. Lu, S. Mori, K. Kobayashi, H. Nanao, Study of tribochemical decomposition of ionic liquids on a nascent steel surface, Appl. Surf. Sci. 255 (2009) 8965, https://doi.org/10.1016/j.apsusc.2009.03.063.
[10] S.S.O. Santos, R.D.S. Millán, M.G. Speziali, Versatile grafted microcrystalline cellulose with ionic liquid as new losartan-controlled release material, Eur. Polym. J. 124 (2020) 109490, https://doi.org/10.1016/j.eurpolymj.2020.109490.
[11] J. Song, Research progress of ionic liquids as lubricants, ACS Omega 6 (2021) 29345, https://doi.org/10.1021/acsomega.1c04512.
[12] W.C. Barnhill, H. Luo, H.M. Meyer, C. Ma, M. Chi, B.L. Papke, J. Qu, Tertiary and quaternary ammonium-phosphate ionic liquids as lubricant additives, Tribol. Lett. 63 (2016) 1, https://doi.org/10.1007/s11249-016-0707-6.
[13] J. Qu, W.C. Barnhill, H. Luo, H.M. Meyer 3rd, D.N. Leonard, A.K. Landauer, B. Kheireddin, H. Gao, B.L. Papke, S. Dai, Synergistic effects between phosphonium-alkylphosphate ionic liquids and zinc dialkyldithiophosphate (zddp) as lubricant additives, Adv. Mater. 27 (2015) 4767, https://doi.org/10.1002/adma.201502037.
[14] W. Li, C. Kumara, H. Luo, H.M. Meyer 3rd, X. He, D. Ngo, S.H. Kim, J. Qu, Ultralow boundary lubrication friction by three-way synergistic interactions among ionic liquid, friction modifier, and dispersant, ACS Appl. Mater. Interfaces 12 (2020) 17077, https://doi.org/10.1021/acsami.0c00980.
[15] P. Lishchuk, A. Vashchuk, S. Rogalsky, L. Chepela, M. Borovyi, D. Lacroix, M. Isaiev, Thermal transport properties of porous silicon filled by ionic liquid nanocomposite system, Sci. Rep. 13 (2023) 5889, https://doi.org/10.1038/s41598-023-32834-8.
[16] H. Fang, Y. Li, S. Zhang, Q. Ding, L. Hu, Novel binary oil-soluble ionic liquids with high lubricating performance, Tribol. Int. 174 (2022) 107724, https://doi.org/10.1016/j.triboint.2022.107724.
[17] F. Xu, H. Li, B. Tian, K. Cui, R. Dong, M. Fan, M. Cai, F. Zhou, W. Liu, Achieving greener, super-robust performance water-based lubrication: obtained by a multifunctional ionic liquid aqueous system and formation of unique interfacial interactions, ACS Sustain. Chem. Eng. 11 (2023) 8651, https://doi.org/10.1021/acssuschemeng.3c01843.
[18] P. Rohlmann, J.J. Black, S. Watanabe, J. Leckner, M.R. Shimpi, M.W. Rutland, J. B. Harper, S. Glavatskih, Tribochemistry of imidazolium and phosphonium bis (oxalato)borate ionic liquids: understanding the differences, Tribol. Int. 181 (2023) 108263, https://doi.org/10.1016/j.triboint.2023.108263.
[19] Y. Lu, S. Watanabe, S. Sasaki, S. Glavatskih, Lubricity of chelated orthoborate-phosphonium ionic liquids on tetrahedral amorphous carbon and steel surfaces, J. Mol. Liq. 378 (2023) 121571, https://doi.org/10.1016/j.molliq.2023.121571.
[20] H. Fang, Y. Li, S. Zhang, Q. Ding, L. Hu, K. Lu, The superior lubricating performance and unique mechanism of oil-soluble protic ionic liquids with short alkyl chains, J. Colloid Interface Sci. 623 (2022) 257, https://doi.org/10.1016/j.jcis.2022.04.174.
[21] Y. Li, S. Zhang, Q. Ding, L. Hu, Effect of cation nature on vacuum tribo-degradation and lubrication performances of two tetrafluoroborate ionic liquids, Tribol. Int. 150 (2020) 106360, https://doi.org/10.1016/j.triboint.2020.106360.
[22] Y. Cao, T. Mu, Comprehensive investigation on the thermal stability of 66 ionic liquids by thermogravimetric analysis, Ind. Eng. Chem. Res. 53 (2014) 8651, https://doi.org/10.1021/ie5009597.
[23] P. Kölle, R. Dronskowski, Synthesis, crystal structures and electrical conductivities of the ionic liquid compounds butyldimethylimidazolium tetrafluoroborate, hexafluorophosphate and hexafluoroantimonate, Eur. J. Inorg. Chem. 2004 (2004) 2313, https://doi.org/10.1002/ejic.200300940.
[24] R. Gusain, P.S. Bakshi, S. Panda, O.P. Sharma, R. Gardas, O.P. Khatri, Physicochemical and tribophysical properties of trioctylalkylammonium bis (salicylato) borate (n888n-bscb) ionic liquids: effect of alkyl chain length, PCCP 19 (2017) 6433, https://doi.org/10.1039/c6cp05990b.
[25] K.I. Hiratsuka, C. Kajdas, Mechanochemistry as a key to understand the mechanisms of boundary lubrication, mechanolysis and gas evolution during friction, Proc. Inst. Mech. Eng., Part J: J. Eng. Tribol. 227 (2013) 1191, https://doi.org/10.1177/1350650113483222.
[26] L. Pisarova, V. Totolin, C. Gabler, N. Dörr, E. Pittenauer, G. Allmaier, I. Minami, Insight into degradation of ammonium-based ionic liquids and comparison of tribological performance between selected intact and altered ionic liquid, Tribol. Int. 65 (2013) 13, https://doi.org/10.1016/j.triboint.2013.02.020.
[27] R.K. Blundell, P. Licence, Tuning cation-anion interactions in ionic liquids by changing the conformational flexibility of the cation, Chem. Commun. 50 (2014) 12080, https://doi.org/10.1039/c4cc05505e.
[28] H. Fang, Y. Li, H. Li, S. Zhang, Q. Ding, W. Yu, L. Hu, Tribological behavior at electronic scales for an oil-soluble ionic liquid with extremely low effective addition and highly load bearing capacity, Chem. Eng. J. 465 (2023) 142810, https://doi.org/10.1016/j.cej.2023.142810.
[29] Y. Li, S. Zhang, Q. Ding, B. Qin, L. Hu, Versatile 4, 6-dimethyl-2-mercaptopyrimidine based ionic liquids as high-performance corrosion inhibitors and lubricants, J. Mol. Liq. 284 (2019) 577, https://doi.org/10.1016/j.molliq.2019.04.042.
[30] C. Gan, T. Liang, W. Li, X. Fan, M. Zhu, Amine-terminated ionic liquid modified graphene oxide/copper nanocomposite toward efficient lubrication, Appl. Surf. Sci. 491 (2019) 105, https://doi.org/10.1016/j.apsusc.2019.06.141.
[31] H. Fang, Y. Li, S. Zhang, Q. Ding, L. Hu, Lubricating performances of oil-miscible trialkylanmmonium carboxylate ionic liquids as additives in PAO at room and low temperatures, Appl. Surf. Sci. 568 (2021) 150922, https://doi.org/10.1016/j.apsusc.2021.150922.
[32] Z. Zheng, X. Liu, H. Yu, H. Chen, D. Feng, D. Qiao, Insight into macroscale superlubricity of polyol aqueous solution induced by protic ionic liquid, Friction 10 (2022) 2000, https://doi.org/10.1007/s40544-021-0563-8.
[33] C.J. Hooke, The elastohydrodynamic lubrication of heavily loaded point contacts, J. Mech. Eng. Sci. 22 (1980) 183, https://doi.org/10.1243/JMES_JOUR_1980_022_036_02.
[34] X. Ge, J. Li, R. Luo, C. Zhang, J. Luo, Macroscale superlubricity enabled by the synergy effect of graphene-oxide nanoflakes and ethanediol, ACS Appl. Mater. Interfaces 10 (2018) 40863, https://doi.org/10.1021/acsami.8b14791.
[35] A.S. Pensado, M.J.P. Comuñas, J. Fernández, The pressure–viscosity coefficient of several ionic liquids, Tribol. Lett. 31 (2008) 107, https://doi.org/10.1007/s11249-008-9343-0.
[36] X. Paredes, O. Fandiño, A.S. Pensado, M.J.P. Comuñas, J. Fernández, Pressure–viscosity coefficients for polyalkylene glycol oils and other ester or ionic lubricants, Tribol. Lett. 45 (2011) 89, https://doi.org/10.1007/s11249-011-9861-z.
[37] M. Björling, S. Bair, L. Mu, J. Zhu, Y. Shi, Elastohydrodynamic performance of a bio-based, non-corrosive ionic liquid, Appl. Sci. 7 (2017) 996, https://doi.org/10.3390/app7100996.
[38] X. Wang, S. Li, F. Guo, X. Li, Numerical simulation of thermo–elastohydrodynamic lubrication of an ionic liquid, Lubr. Eng. 45 (2020) 45, https://doi.org/10.3969/j.issn.0254-0150.2020.02.009.